Graphene hybridized polydopamine-kaolin composite as effective adsorbent for methylene blue removal

Kai He[1], Guangming Zeng[1,*], Anwei Chen[2,*], Zhenzhen Huang[1], Min Peng[1], Tiantian Huang[1], Guiqiu Chen[1].

1. *College of Environmental Science and Engineering, Hunan University and Key Laboratory of Environmental Biology and Pollution Control (Hunan University), Ministry of Education, Changsha 410082, PR China*

2. *College of Resources and Environment, Hunan Agricultural University, Changsha 410128,PR China*

For corresponding authors at: E-mail addresses: zgming@hnu.edu.cn (G. Zeng), A.Chen@hunau.edu.cn (A. Chen). Tel.: +86 731 88822829; fax: +86 731 88823701.

Abstract: To explore the approach for further enhancing the dye removal performance of polydopamine (PDA) coated materials, a novel composite of PDA-kaolin with reduced graphene oxide hybridization (PDA-rGO-kaolin) was synthesized and selected as a model adsorbent for methylene blue (MB) removal. The BET characteristic analysis showed that the introduction of rGO significantly increased the surface area of PDA-kaolin by 3.1 times. A series of comparative experiments on PDA-kaolin and PDA-rGO-kaolin towards MB removal in various conditions were carried out. Adsorption experiment indicated that PDA-rGO-kaolin was more satisfactory for MB removal. Kinetic analysis showed that the adsorption followed a pseudo-second-order kinetic model. The adsorption behavior could be better described by Langmuir isotherm model. Compared with PDA-kaolin, PDA-rGO-kaolin showed higher maximum adsorption capacity towards MB (39.663 mg/g). Furthermore, the adsorption of MB molecules on adsorbents was spontaneous and endothermic process according to thermodynamic experiment. Moreover, PDA-rGO-kaolin showed a good regeneration performance for MB removal. These results show that the introduction of graphene is a feasible and efficient method to improve the adsorption performance of PDA coated kaolin composite.

Keywords: Polydopamine; Reduced graphene oxide; Kaolin; Methylene blue; Adsorption performance.

Introduction

Environment pollution is one of the most urgent problems worldwide. The elimination of various contaminants, such as aromatic pollutants[1-3], heavy metals[4-7], and organic dyes[8-11], in environment is vital for ecosystem and human health. To date, the common technologies employed for the removal of these contaminants include adsorption[12-15], membrane filtration[16], oxidative process[17-19], and biological treatment[20-22]. Among these mentioned approaches, adsorption has been regarded as an efficient and attractive method in pollutant removal due to its properties of low-cost, high-efficiency, and easy-design[23,24]. Organic dyes are the most abundant, visible, and hazardous contaminants in wastewater, which can impede the penetration of sunlight and endanger the survival of aquatic organisms[10, 25-28]. Therefore, the dye removal from water bodies is necessary. Currently, kaolin, one of the common clay minerals, has been used as adsorbent for wastewater treatment[29]. Compared with other commercial or synthetic adsorbents[11,30,31], the application of kaolin has advantages in terms of low-cost, abundant availability, and eco-friendly, which can bring vast economic and environmental benefits to wastewater industries[32]. Nonetheless, the application of kaolin alone in wastewater treatment may not be satisfactory due to its relative low adsorption capacity[29,33]. This low adsorption efficiency of methylene blue (MB) on kaolin has also been observed in our previous work[34]. Thus, it is necessary to seek efficient strategy to activate kaolin.

Mussel-inspired chemistry is an emerging strategy for the surface modification on various solid materials[35]. A number of studies have demonstrated that polydopamine (PDA) coating, the self-polymerization of dopamine in alkaline or oxidants, is a universal surface functionalization agent to various materials. For example, Cheng et al. (2013) explored the performance of PDA coated graphene in 2D and 3D architectures as adsorbents in pollutant disposal[36]. Yan et al. (2015) prepared PDA coated electrospun poly(vinyl alcohol)/poly(acrylic acid) membranes and found that the as-prepared membranes exhibited efficient adsorption performance towards methyl blue[37]. Zhang et al. (2014) synthesized PDA decorated magnetic nanoparticles (Fe_3O_4/PDA) and applied the as-prepared materials for the removal of multiple pollutants in environmental remediation[38]. Yu et al. (2014) successfully prepared PDA coated zeolite powder at different reaction time and investigated the removal performance towards copper ions[39]. Huang et al. (2016) utilized PDA coating as a platform to further conjugate with poly-(sodium p-styrenesulfonate hydrate) (PSPSH) on the surface of kaolin. They examined the removal of MB by the as-prepared functionalized kaolin, while a comparative study towards the PDA modified kaolin was missed[29]. In our study, we firstly demonstrated that the removal of MB was significantly enhance by kaolin with PDA modification. These results collectively showed that mussel-inspired modification indeed could enhance the wastewater treatment performance. However, the PDA coating may decrease the surface area of material, which will impede the application of PDA and decrease the maximum removal capacity towards pollutants in some extent[36,39]. In order to minimize its drawbacks and maximize its application potential, therefore, it is important to explore a feasible approach to further improve the wastewater treatment performance of PDA coated materials.

Excitingly, the discovery of graphene opens up a new opportunity to solve the above-mentioned problems. As is well known, graphene materials have been widely applied in environmental fields due to their unique physicochemical properties[40-42]. Importantly, the graphene modification can greatly enhance the pollutant removal performance[43,44]. However, the synthesis of graphene usually involves the use of toxic or hazardous reducing agents in the reduction of graphene oxide[45]. Thus, a green approach for the graphene synthesis is necessary. Herein, dopamine can act as not only an environmental-friendly reducing agent for preparing graphene but also a capping agent to decorate the resulting material. However, the studies on the modification of graphene and dopamine on clay materials are limited. Thus, the application of PDA-reduced graphene oxide as surface capping agent on kaolin in the wastewater treatment is worth exploring.

In this study, the main objective was to explore the approach for further enhancing dye removal by PDA modified material. Thus, reduced graphene oxide modified kaolin with PDA coating (PDA-rGO-kaolin) was successfully prepared. Moreover, a comparative experiment was carried out to investigate the removal performance of PDA-kaolin and PDA-rGO-kaolin towards dye removal. Batch experiments were conducted to compare the adsorption process and behavior of both PDA-kaolin and PDA-rGO-kaolin towards MB at different solution conditions. We deem that this work will provide a theoretical basis for the design and application of novel PDA-coated materials in environmental field.

Materials and methods

Materials

Graphene oxide (GO) was firstly prepared according to the modified Hummers method, which was used for the synthesis of reduced graphene oxide [34,46]. Kaolin ($Al_2Si_2O_9H_4$), 3-aminopropyl-trimethoxysilane (APTMS) as linkage, dopamine hydrochloride (DA) as reductant and wrapping agent, tris(hydroxymethyl) aminomethane (Tris), MB, and all other chemicals were purchased from Sinopharm chemical reagent Co., Ltd, China. Distilled water was used for the preparation of solutions in all experiments.

Synthesis of PDA-rGO-kaolin composites

In order to obtain the PDA-rGO-kaolin composites, the GO-kaolin composites (3:20, w/w) were prepared firstly according to our previous study [34]. Then, the obtained GO-kaolin composite (1 g) and 500 mg DA were immersed into 250 mL of 10 mM Tris-HCl solution (pH=8.5) and dispersed by sonication for 30 min. Afterwards, the mixture was stirred vigorously at 60 ℃ for the reduction of GO for 24 h, and the resultant black PDA-rGO-kaolin was filtered and washed with distilled water for several times and dried in a vacuum oven at 50 ℃ for 24 h [45,47]. The PDA coated kaolin was prepared by mixing DA and kaolin without the interaction of GO.

Characterizations

The surface morphology and chemical compositions of PDA-kaolin and PDA-rGO-kaolin composites were characterized using Transmission Electron Microscope (TEM) (JEOL, Japan) and X-ray photoelectron spectroscopy (XPS) on ESCALAB 250Xi (Thermo Fisher Scientific, USA), respectively. The specific surface area was measured based on Brunauer-Emmett-Teller (BET) method using nitrogen as absorbent. Thermogravimetric analysis (TGA) was carried out using thermoanalytical equipment (SDT Q600, USA) at a heating ratio of 10 ℃/min from 20 to 800 ℃ at nitrogen atmosphere. Raman spectra were obtained on a LabRam-010 Raman spectrometer (Jobin Yvon, French); the laser excitation was provided by an Ar+ laser at a wavelength of 514 nm. The zeta potentials of samples in solution under different pH conditions were measured by a zeta potential meter (Zetasizer Nano-ZS90, Malvern).

Adsorption experiments

The basic dye, MB was chosen as the model pollutant and a 500 mg/L of MB stock solution was prepared for the following adsorption experiments. In order to measure the dye concentration, a standard curve of MB solution was obtained at 664 nm by using a UV–vis spectrophotometer (UV-2550, SHIMADZU, Japan). Batch adsorption experiments were carried out by adding 40 mg adsorbent into 50 mL MB solution and shaken for 24 h (180 rpm, 27 ± 1 ℃) at a water bath shaker. The suspensions were then filtered through 0.45 μm membrane filter to measure the final dye concentration. The effect of initial dye concentrations varied from 5 to 40 mg/L was investigated and an initial dye concentration of 20 mg/L was chosen for the following experiments. The effects of solution pH (3.5 to 11.0), adsorbent dosage (0.4 to1.6 g/L), and temperatures of solution at the desired values (17, 27, 37, and 47 ℃) on the MB removal were studied. To analyze the experiment data, the removal efficiency (R) and adsorption capacity (Q_e (mg/g)) of PDA-kaolin and PDA-rGO-kaolin composites towards MB were calculated according to following equations, respectively:

$$R=\frac{C_0\text{-}C_e}{C_0}\times 100\% \quad (1)$$

$$Q_e=\frac{(C_0\text{-}C_e)}{m}\times V \quad (2)$$

where C_0 and C_e are the initial and equilibrium concentrations (mg/L) of MB in solution, respectively. V (L) and m (g) represent the volume of dye solution and the mass of adsorbent used in the dye solution.

Results and discussion

Characterization of PDA-kaolin and PDA-rGO-kaolin

In this work, PDA-rGO-kaolin material was synthesized through a two-step route. Previously, the GO sheets were attached to APTMS modified kaolin due to electrostatic interactions [47]. Afterward, the reduction of GO to rGO occurred after the addition of dopamine as reduction agent. Simultaneously, PDA-rGO-kaolin composite was formed due to the self-polymerization of dopamine to PDA [45].

According to previous studies[29,45], the potential synthetic process is presented in Scheme 1. As the low adsorption performance of raw kaolin on MB solution has been demonstrated in our previous work [34], thus we focused on the comparison of dye removal performance between PDA-kaolin and PDA-rGO-kaolin as adsorbents in this study.

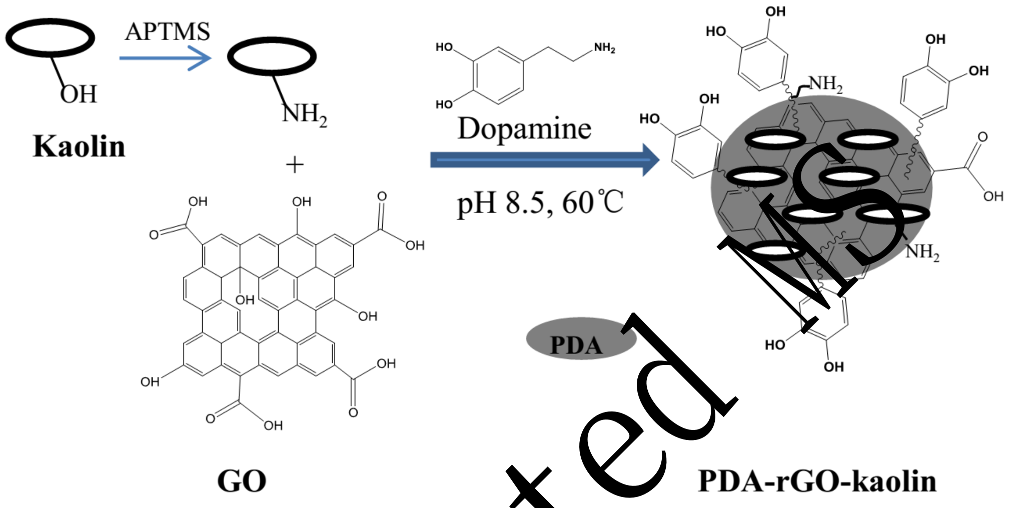

Scheme 1. Synthetic process of PDA-rGO-kaolin composite.

After coating treatments, the surface changes of kaolin could be observed by TEM images as shown in Fig.1. Obviously, a narrow covering layer could be observed in the surface of kaolin (Fig. 1a) after PDA coating (Fig. 1b), which confirmed the successful self-polymerization of dopamine onto the surface of kaolin [33,38]. Fig. 1c presented the corresponding TEM image of PDA-rGO-kaolin. The surrounding sheets (shown in red circle) were obvious, which did not appear in other images, demonstrating the successful contact of graphene sheets with kaolin flakes [45]. The graphene sheets could support a large surface area for kaolin, which was verified by the measurement of BET surface area. Compared with the surface area of raw kaolin powder (9.65 m^2/g), the surface area of PDA-kaolin composite decreased to 8.62 m^2/g.

The decrease of surface area by PDA coating was also reported in PDA-zeolite particles [39]. In contrast, the surface area of PDA-rGO-kaolin increased significantly to 35.35 m^2/g, increased by 3.1 folds in comparison with that of PDA-kaolin. These results revealed that the graphene modification could improve the limitation of PDA coating.

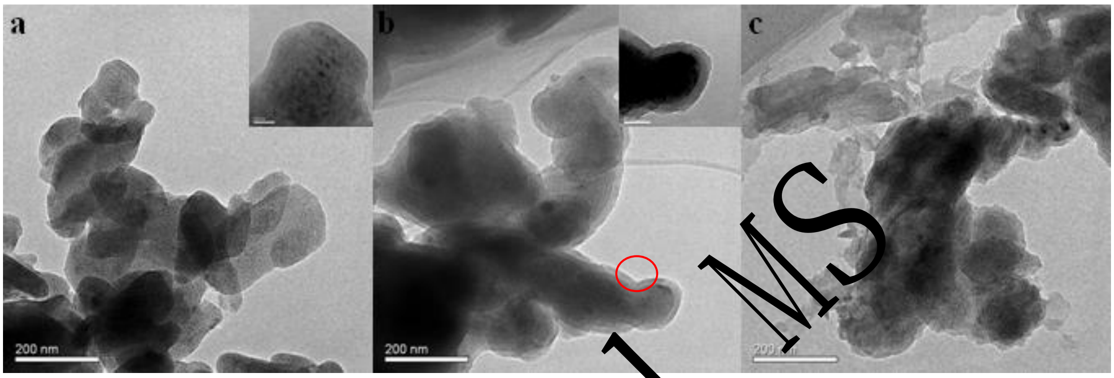

Fig. 1. TEM images of raw kaolin (a), PDA-kaolin (b), and PDA-rGO-kaolin (c). Insets (a, b): the corresponding TEM images with high magnification.

From the TGA curves in Fig. 2a, it could be seen that raw kaolin presented only 1.59% weight loss at 800 ℃. The weight loss in raw kaolin was attributed to the weight loss of hydroxyl groups or adsorbed gases on kaolin [48]. The weight loss of PDA-kaolin increased to 10.33% after the surface modification of kaolin with PDA, owing to the decomposition of PDA from the PDA-kaolin surface [39,49]. Distinct weight loss (27.78%) of PDA-rGO-kaolin was observed due to the thermal decomposition of labile oxygen-containing groups on graphene as reported in previous studies [50-52]. The differences of TGA curves suggested the successful PDA and PDA-rGO coating on the kaolin surface. Raman spectra can be used as a sensitive detection method to determine the chemical structure of carbonaceous materials. Fig. 2b showed the Raman spectra of PDA-kaolin and PDA-rGO-kaolin composites. Compared with PDA-kaolin, a relatively obvious D band was observed on the Raman spectrum of PDA-rGO-kaolin composite. It has been reported that the D band represents the sp^3 defects in carbon[43], indicating the successful introduction of rGO in composite combining with the XPS analysis.

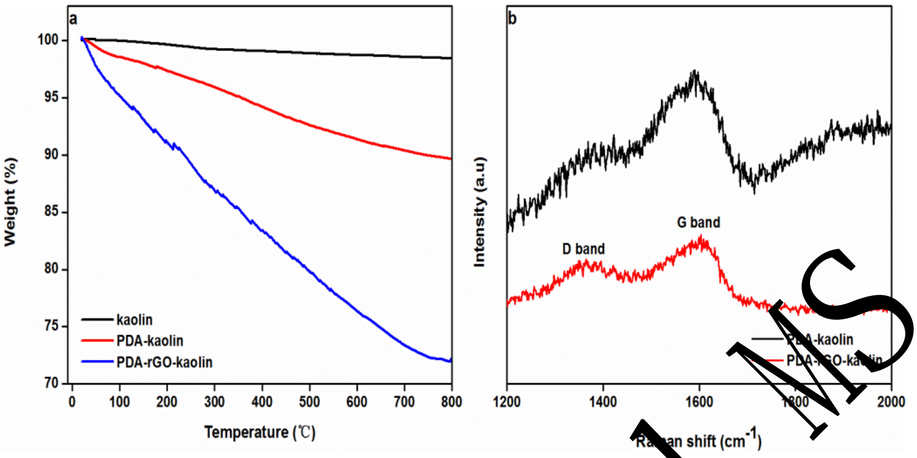

Fig. 2. (a) TGA analysis of raw kaolin, PDA-kaolin, and PDA-rGO-kaolin composites; (b) Raman spectra of PDA-kaolin and PDA-rGO-kaolin composites.

In addition, the element compositions and main functional groups were analyzed by XPS measurement, which could further verify the successful coating. As shown in survey scan of XPS spectra (Fig. 3a) and component analysis (Table 1), the typical characteristic elements of kaolin such as Al, Si, and O were observed in the modified kaolin composites. However, the peaks of Si and Al nearly disappeared owing to the PDA coating inhibited the penetration of XPS, indicating that the surface of kaolin was fully covered by PDA polymer [38]. In addition, a new peak at ~399 eV corresponding to N1s element was observed in the XPS spectra of modified kaolin, indicating the growth of PDA polymer on the surface of kaolin [39]. To further understand the relative contents of core groups, the C1s spectra of PDA-kaolin and

PDA-rGO-kaolin were deconvoluted into several peak components (Fig. 3b). The C1s core-level spectrum of PDA-kaolin can be curved into four peak components at 284.6, 285.3, 286.1, and 288.0 eV, which signified the presence of C–C, C–N, C–O, and C=O groups, respectively [45,52]. The appearance of O–C=O peak component at 288.8 eV in the C1s core-level spectrum of PDA-rGO-kaolin was derived from the partially reduced GO [45]. Furthermore, the ratio of C–C group and the percentage of C atom on PDA-rGO-kaolin were higher than that on PDA-kaolin, which also indicated that graphene sheets were introduced into kaolin composite.

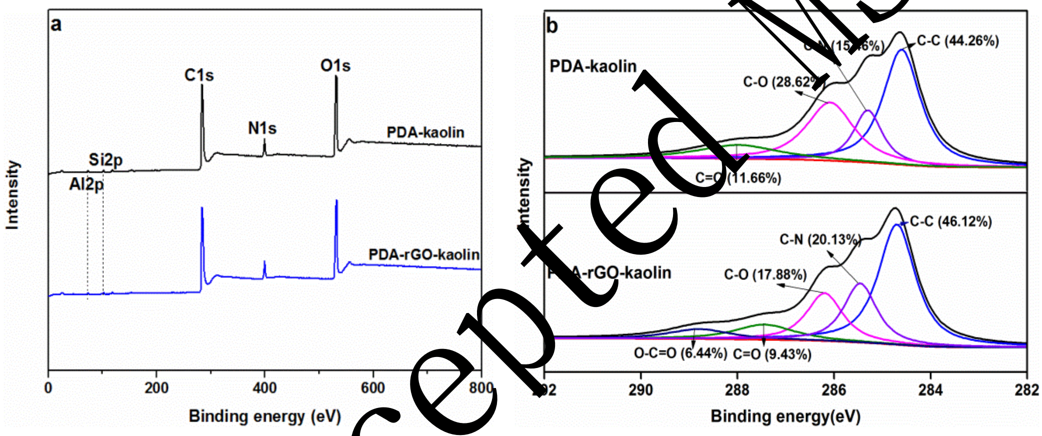

Fig. 3. XPS survey (a) and C1s core-level spectra (b) of PDA-kaolin and PDA-rGO-kaolin samples.

Table 1 Element compositions and atom ratios of PDA-kaolin and PDA-rGO-kaolin samples

Samples	Atom percentage (%)				
	C1s	N1s	O1s	Si2p	Al2p
PDA-kaolin	64.055	7.536	25.563	1.818	1.989
PDA-rGO-kaolin	65.269	7.849	23.755	1.457	1.671

Effect of contact time and adsorption kinetics

It could be observed from the Fig. 4 that the removal efficiency and adsorption capacity of PDA-rGO-kaolin were higher than that of PDA-kaolin. As seen from Fig. 4a, the adsorption rate became slow gradually with time until a state of equilibrium was acquired. Nevertheless, the adsorption of MB by PDA-rGO-kaolin was more rapid than that by PDA-kaolin at the initial stage, and the application of PDA-rGO-kaolin could shorten the needed time to reach equilibrium. The enhanced dye adsorption by PDA-rGO-kaolin was ascribed to its higher surface area and more available surface active sites for adsorption[53]. The results indicated that the introduction of rGO was beneficial for the adsorption of MB molecules on kaolin composite.

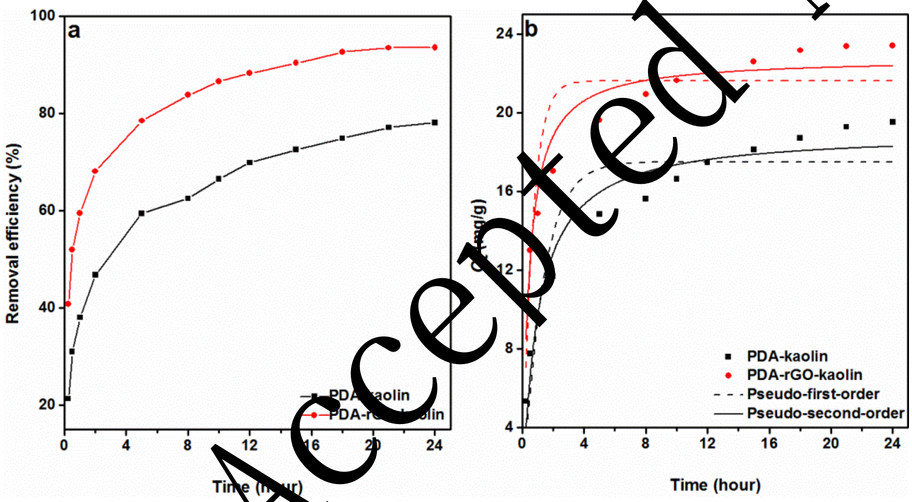

Fig. 4. Effect of contact time on MB removal (20 mg/L, pH=7.0) by PDA-kaolin and PDA-rGO-kaolin at 27 ℃ (a). The fitted kinetics models from experiment data: the dash lines and solid lines represent pseudo-first-order and pseudo-second-order models, respectively (b).

Commonly, pseudo-first-order and pseudo-second-order kinetic models are used to analyze the adsorption process. The fitted kinetic curves (Fig. 4b) obtained from experiment data were based on two non-linear forms as Eqs (3) and (4), respectively:[33]

$$Q_t = Q_e(1\text{-}e^{k_1 t}) \qquad (3)$$

$$Q_t = \frac{k_2 Q_e^2 t}{1+k_2 Q_e t} \qquad (4)$$

where Q_t (mg/g) and Q_e (mg/g) are the adsorption capacity of adsorbent towards dye solution at different contact time (t) and equilibrium time, respectively. k_1 (h^{-1}) and k_2 (g mg^{-1} h^{-1}) are the pseudo-first-order and pseudo-second-order rate constant, respectively.

Table 2 Kinetic parameters for the adsorption of MB onto PDA-kaolin and PDA-rGO-kaolin

Samples	Pseudo-first-order			Pseudo-second-order		
	$Q_{e(\mathrm{cal})}$ (mg/g)	k_1 (h^{-1})	R^2	$Q_{e(\mathrm{cal})}$ (mg/g)	k_2 (g mg^{-1} h^{-1})	R^2
PDA-kaolin	17.51	0.7845	0.860	19.03	0.0548	0.950
PDA-rGO-kaolin	21.64	1.5355	0.780	22.78	0.1042	0.933

The kinetic parameters including correlation coefficients (R^2), k_1, k_2, and calculated $Q_{e(\mathrm{cal})}$ are displayed in Table 2. Obviously, the pseudo-second-order kinetic model for the adsorption on PDA-kaolin and PDA-rGO-kaolin showed better regression coefficient for the kinetic data (R^2 = 0.950 and 0.933, respectively) than pseudo-first-order kinetics model (R^2 = 0.860 and 0.780, respectively). Thus, the adsorption of MB on composites could be better described by the pseudo-second-order model. According to the assumption of pseudo-second-order kinetic model[29,54], it inferred that the removal of MB by PDA-kaolin and PDA-rGO-kaolin adsorbents might be chemical adsorption [55].

Effect of initial dye concentration

To investigate the effect of initial dye concentration on the removal of MB, the adsorbent dosage was set as 0.8 g/L. As shown in Fig. 5, similar decreasing trends of MB removal were observed. At higher initial MB concentration, PDA-kaolin and PDA-rGO-kaolin could get lower removal efficiency. The dye removal for 5–40 mg/L of MB was 84.32%–50.77% by PDA-kaolin. However, the corresponding MB removal efficiency reached 97.28%–77.13% at same MB concentration using PDA-rGO-kaolin as adsorbent. Generally, MB molecules at higher concentration solution will occupy more active sites on the adsorbents and cause the saturation of active sites, thereby reducing the adsorption efficiency [21,56].

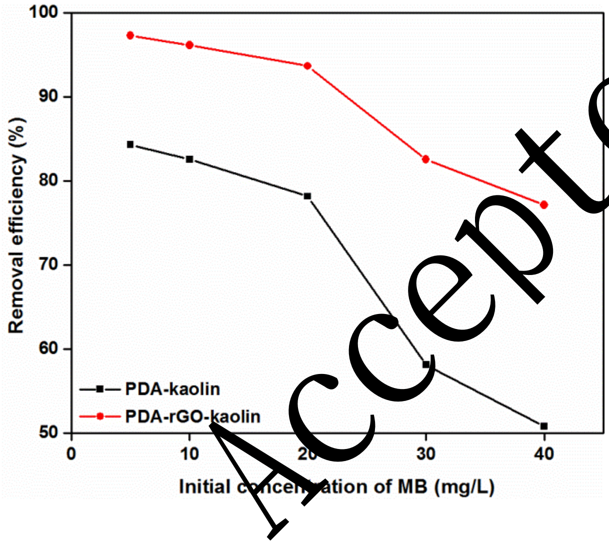

Fig. 5. Effect of initial dye concentration on the MB removal by PDA-kaolin and PDA-rGO-kaolin composites.

Effect of adsorbent dosage

An increased trend of dye removal with the increase of adsorbent dosage was observed from Fig. 6. Compared with the low dosage of adsorbent, high dosage of adsorbent possessed larger surface area and provided more adsorption sites at constant dye concentration, resulting in a lower dye concentration residual in the solution[12].

The removal efficiency of MB has already reached 93.66% by PDA-rGO-kaolin at a dosage of 0.8 g/L, whereas only 78.16% of MB was removed by PDA-kaolin at the same adsorbent dosage. Even if the PDA-kaolin dosage increased to 1.6 g/L, the removal efficiency of MB was still lower (about 90%) than that of PDA-rGO-kaolin at 0.8 g/L. Apparently, the dye removal by PDA-rGO-kaolin was more superior than that by PDA-kaolin.

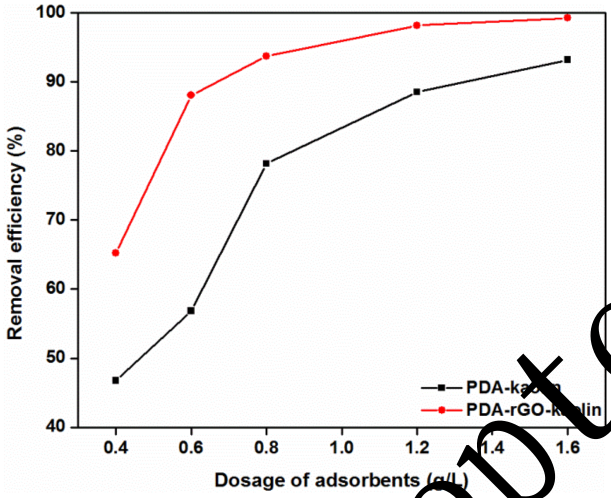

Fig. 6. Effect of adsorbent dosage on the removal of MB.

Effect of solution pH

The removal of MB by PDA-kaolin and PDA-rGO-kaolin was investigated at the dye solution pH in the range of 3.5–11.0. As shown in Fig. 7a, the removal efficiency of MB by PDA-kaolin and PDA-rGO-kaolin showed a similar increase trend with the increase of pH, which is in agreement with other reports[38,57]. The increased adsorption suggested that one of the contributions to adsorption resulted from electrostatic attraction between adsorbent and dye molecules[58]. As seen from Fig. 7b, the zeta potentials of PDA-kaolin and PDA-rGO-kaolin under varied pH solution were determined. For cationic dye, the adsorbent surface with more negative charge should have a higher removal efficiency of MB. However, PDA-rGO-kaolin with lower negative charge adsorbed more MB molecules, which might be ascribed to the strong π-π interactions between rGO and MB molecules in addition to electrostatic attraction.[34] Thus, the proposed adsorption mechanism of MB molecules on PDA-rGO-kaolin is illustrated in Scheme 2[41,52,53]. In summary, the adsorption of MB was pH-dependent and the increase of solution pH was beneficial to the adsorption of MB on PDA-kaolin samples.

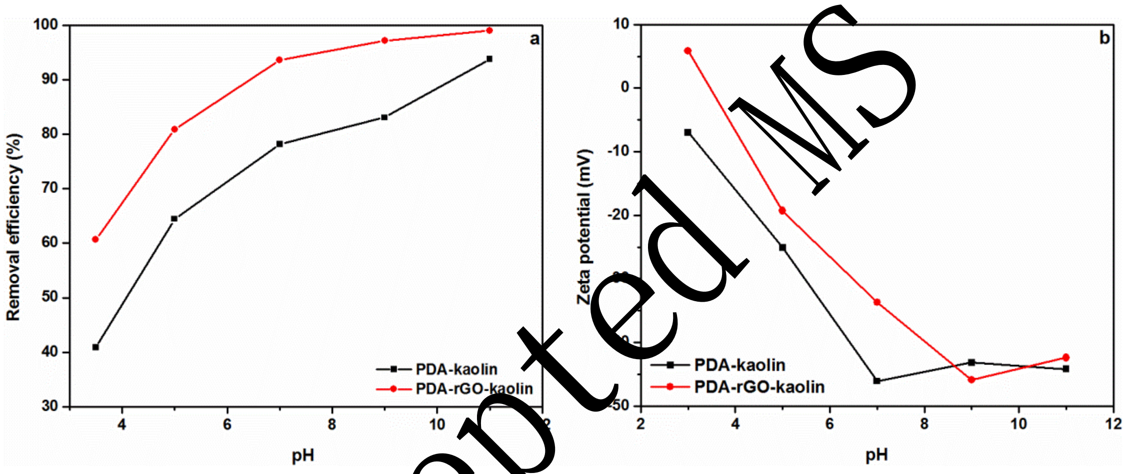

Fig. 7. (a) Effect of solution pH on the removal of MB by PDA-kaolin and PDA-rGO-kaolin composites, and (b) Zeta potentials of PDA-kaolin and PDA-rGO-kaolin at varied pH solution.

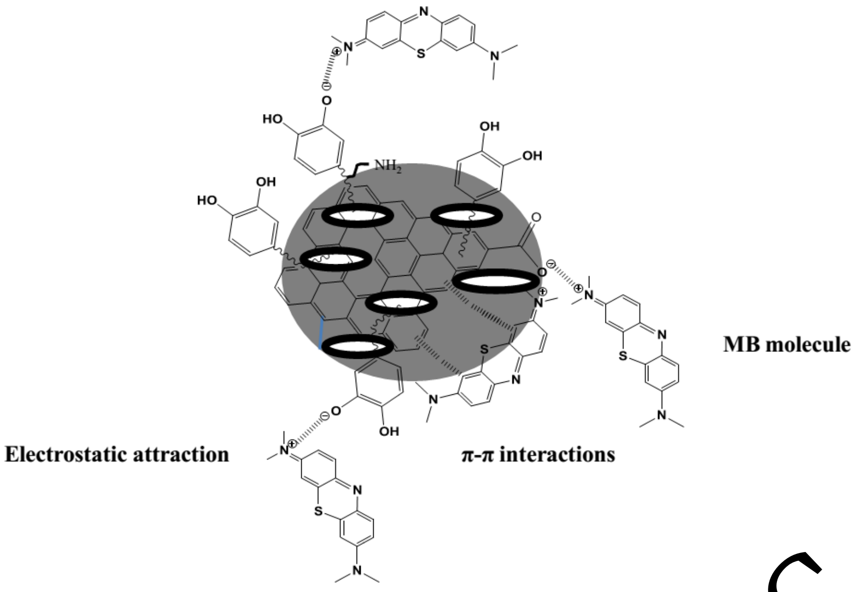

Scheme 2. Proposed adsorption mechanism of MB molecules on PDA-rGO-kaolin composite.

Effect of temperature and adsorption thermodynamics

Thermodynamic experiment result (Fig. 8a) showed that higher temperature was favorable for the adsorption of MB by PDA-kaolin and PDA-rGO-kaolin. This result indicated that the adsorption reactions were endothermic in nature.

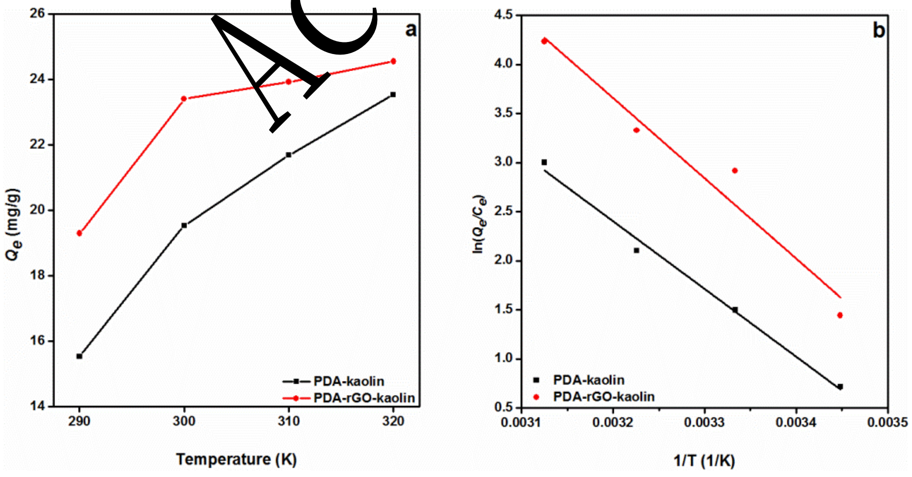

Fig. 8. Effect of temperature on the adsorption of MB by PDA-kaolin and PDA-rGO-kaolin samples: adsorption capacity at different temperatures (a) and

thermodynamic analysis (b).

Several important thermodynamic parameters change in Gibb's free energy (ΔG^0), entropy (ΔS^0) and enthalpy (ΔH^0) are calculated from the following equations [59].

$$\ln K_d = \frac{\Delta S^0}{R} - \frac{\Delta H^0}{RT} \qquad (5)$$

$$\Delta G^0 = \Delta H^0 - T\Delta S^0 \qquad (6)$$

where K_d is calculated from Q_e/C_e. T is absolute temperature in Kelvin (K), and R is the universal gas constant (8.314 kJ/(mol K)). ΔH^0 and ΔS^0 are determined from the slope and intercept of the Van't Hoff plots of $\ln K_d$ versus of 1/T (Fig. 8b), respectively.

Table 3 Thermodynamic parameters for the adsorption of MB onto PDA-kaolin and PDA-rGO-kaolin samples

Samples	Temperature (K)	ΔG^0 (kJ/mol)	ΔH^0 (kJ/mol)	ΔS^0 (kJ/(K mol))
PDA-kaolin	290	-1.773	57.387	0.204
	300	-3.813		
	310	-5.835		
	320	-7.893		
PDA-rGO-kaolin	290	-3.898	68.022	0.248
	300	-6.378		
	310	-8.858		
	320	-11.338		

As listed in Table 3, the changes of thermodynamic parameters could be observed. The decreasing trend of ΔG^0 values with the increase of temperature indicated that higher temperature was more favorable for the adsorption. The negative value of ΔG^0

and positive values of ΔH^0 suggested that the adsorption process of MB onto two adsorbents was spontaneous and endothermic process. Furthermore, the positive values of ΔS^0 reflected some structural changes in dye and adsorbents and implied the increased degrees of the randomness at the adsorbate-adsorbent interface during the adsorption[29,60].

Adsorption isotherms

Adsorption isotherms, especially the two common isotherm models such as Freundlich and Langmuir isotherms, play important roles in depicting the interaction pathway to solid-solution adsorption system[29,53,61]. These two models can be expressed in non-linear forms as follows:

$$Q_e = K_F C_e^{1/n}$$

(7)

$$Q_e = \frac{Q_m K_L C_e}{1 + K_L C_e}$$

(8)

where K_F [(mg/g)(L/mg)$^{1/n}$] and n are the adsorption equilibrium constant of Freundlich isotherm model. The Q_m (mg/g) and K_L (L/mg) are the theoretical maximum adsorption capacity of adsorbent and Langmuir isotherm constant, respectively. The fitted curves of Langmuir and Freundlich isotherms could be seen from Fig. 9.

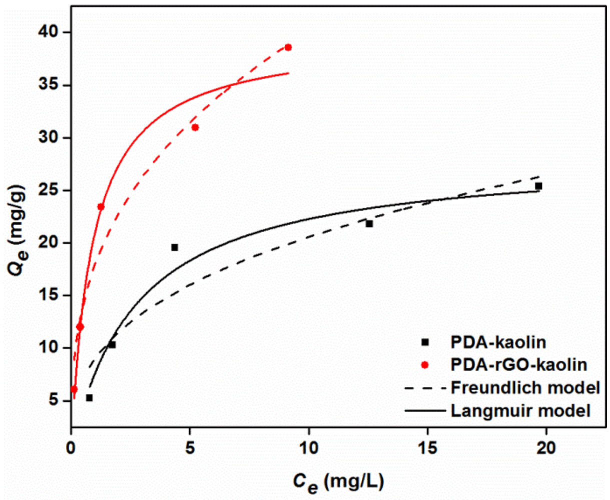

Fig. 9. Adsorption isotherms of MB by PDA-kaolin and PDA-rGO-kaolin samples; the data from experiment have been fitted by Langmuir (solid lines) and Freundlich (dash lines) isotherm models.

Table 4 Parameters of adsorption isotherms for MB onto PDA-kaolin and PDA-rGO-kaolin samples

Samples	Freundlich model			Langmuir model		
	K_F [(mg/g)(L/mg)$^{1/n}$]	$1/n$	R^2	Q_m (mg/g)	K_L (L/mg)	R^2
PDA-kaolin	8.944	0.361	0.864	28.414	0.362	0.960
PDA-rGO-kaolin	17.867	0.351	0.952	39.663	1.114	0.971

According to the correlation coefficient of these two fitted models in Table 4, it can be found that the experiment data was better fitted by Langmuir isotherm models than Freundlich isotherm models. Besides, the calculated Q_m values from Langmuir isotherm models for PDA-kaolin (28.411 mg/L) and PDA-rGO-kaolin (39.663 mg/L) were more close to the corresponding experiment data (25.385 and 38.565 mg/L, respectively). It also indicated that the adsorption of MB on adsorbents was better explained by Langmuir model. Furthermore, by comparison of the maximum adsorption capacities obtained in this study with some previously reported studies of various adsorbents for MB removal (Table 5), it can be inferred that the as-prepared PDA-rGO-kaolin adsorbent was better than many other adsorbents. However, the adsorption capacity of PDA-rGO-kaolin composite towards MB solution was still not high. Therefore, more efforts should paid to improve the application of modified clay materials as adsorbents in wastewater treatment.

Table 5 Maximum adsorption capacity (Q_m) of MB by various adsorbents in other reports

Adsorbents	Q_m (mg/g)	References
Raw kaolin	13.99	[57]
Zeolite	22	[12]
Magnetic multi-wall carbon nanotube	15.87	[58]
Biochar	8	[44]
Graphene coated biochar	174	
Bentonite	151~175	[50]
Kaolin-GO	28.016	[34]
PDA-rGO-kaolin	39.663	In this study

Regeneration performance

The regeneration performance of an adsorbent is necessary for its practical application in terms of economical benefits. According to the above results, PDA-rGO-kaolin adsorbent was selected to investigate the potential regeneration ability for MB removal due to its higher adsorption capacity towards MB. After adsorption, the adsorbent was put into acidic ethanol solution under stirring for 30 min, followed by filtration and washing processes to remove MB. Then, the adsorbent was dried and used for the next cycle of adsorption experiment. The regeneration performance of PDA-rGO-kaolin adsorbent is presented in Fig. 10a. The adsorption efficiency was gradually declined with the proceed of regeneration experiment, which was similar with previous reports due to the loss of active adsorption sites[29,34]. However, the adsorption efficiency of MB after five cycles still remained 84%. Therefore, the application of PDA-rGO-kaolin as adsorbent for dye removal showed good regeneration performance.

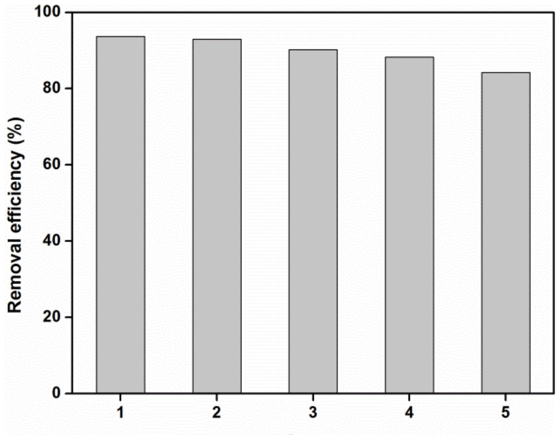

Fig. 10. Adsorption of MB on PDA-rGO-kaolin in five cycles.

Conclusions

In this study, the PDA and reduced graphene oxide modified kaolin composite (PDA-rGO-kaolin) was successfully prepared by a facile method, and this composite showed excellent dye removal performance. The adsorption results suggested that the adsorption of MB by the PDA-rGO-kaolin was obviously more superior than that by PDA-kaolin. The enhancement of MB removal was attributed to the increased surface area and adsorption active sites. Furthermore, the increase of solution pH could enhance the adsorption of MB. The kinetic and isotherm fitted curves indicated that the adsorption could be better described by pseudo-second-order kinetics model and Langmuir isotherm model, respectively. Additionally, the adsorption was favorable at higher temperature. PDA-rGO-kaolin as adsorbent showed a good regeneration performance for MB removal. Findings of this work can provide a basis for further designing novel PDA coated clay materials for various environmental applications. On the other hand, this as-prepared composite was difficult to be separated from aqueous solution, thus much work should be conducted to improve the practical application in future research.

Acknowledgements

This study was financially supported by the National Natural Science Foundation of China (51521006 and 51508186), the Program for Changjiang Scholars and Innovative Research Team in University (IRT-13R17), the Hunan Provincial Natural Science Foundation of China (2016JJ3076).

Conflict of interest

The authors declare that they have no conflict of interest.

References

[1] Xiao P, Wang P, Li H, Li Q, Shi Y, Wu XL, et al. New insights into bisphenols removal by nitrogen-rich nanocarbons: Synergistic effect between adsorption and oxidative degradation. J Hazard Mater 2018; 345:123–130.

[2] Zhou C, Lai C, Huang D, Zeng G, Zhang C, Cheng M, et al. Highly porous carbon nitride by supramolecular preassembly of monomers for photocatalytic removal of sulfamethazine under visible light driven. Appl Catal B Environ 2018;220:202–10.

[3] Wang P, Xiao P, Zhong S, Chen J, Lin H, Wu XL. Bamboo-like carbon nanotubes

derived from colloidal polymer nanoplates for efficient removal of bisphenol A. J. Mater. Chem. A 2016;4:15450-6.

[4] Liang J, Yang Z, Tang L, Zeng G, Yu M, Li X, et al. Changes in heavy metal mobility and availability from contaminated wetland soil remediated with combined biochar-compost. Chemosphere 2017;181:281–8.

[5] Wan J, Zeng G, Huang D, Hu L, Xu P, Huang C, et al. Rhamnolipid stabilized nano-chlorapatite: Synthesis and enhancement effect on Pb-and Cd-immobilization in polluted sediment. J Hazard Mater 2018;343:332–9.

[6] Jamshidi M, Ghaedi M, Dashtian K, Hajati S. New ion-imprinted polymer-functionalized mesoporous SBA-15 for selective separation and preconcentration of Cr(III) ions: modeling and optimization. Rsc Adv 2015;5:105789–99.

[7] Azad FN, Ghaedi M, Dashtian K, Jamshidi A, Hassani G, Montazerozohori M, et al. Preparation and characterization of an AC–Fe_3O_4–Au hybrid for the simultaneous removal of Cd^{2+}, Pb^{2+}, Cr^{3+} and Ni^{2+} ions from aqueous solution via complexation with 2-((2,4-dichloro-benzylidene)-amino)-benzenethiol: Taguchi optimization. Rsc Adv 2016;6:19780–91.

[8] Deng J, Zhang X, Zeng G, Gong J, Niu Q, Liang J. Simultaneous removal of Cd (II) and ionic dyes from aqueous solution using magnetic graphene oxide nanocomposite as an adsorbent. Chem Eng J 2013;226:189–200.

[9] Tehrani-Bagha AR, Nikkar H, Mahmoodi NM, Markazi M, Menger FM. The sorption of cationic dyes onto kaolin: Kinetic, isotherm and thermodynamic studies. Desalination 2011;266:274–80.

[10] He K, Chen G, Zeng G, Chen A, Huang Z, Shi J, et al. Three-dimensional

graphene supported catalysts for organic dyes degradation. Appl Catal B Environ 2018; 228:19–28.

[11] Shi YC, Wang AJ, Wu XL, Chen JR, Feng JJ. Green-assembly of three-dimensional porous graphene hydrogels for efficient removal of organic dyes. J. Colloid Interface Sci. 2016; 484:254–262.

[12] Rida K, Bouraoui S, Hadnine S. Adsorption of methylene blue from aqueous solution by kaolin and zeolite, Appl. Clay Sci. 2013; s83–84:99–105.

[13] Xu P, Zeng GM, Huang DL, Feng CL, Hu S, Zhao MH, et al. Use of iron oxide nanomaterials in wastewater treatment: a review. Sci Total Environ 2012;424:1–10.

[14] Zhang C, Lai C, Zen, G, Huang D, Yang C, Wang Y, et al. Efficacy of carbonaceous nanocomposites for sorbing ionizable antibiotic sulfamethazine from aqueous solution., Water Res. 2016; 95:103–112.

[15] Ghaedi M, Azad FN, Dashtian K, Hajati S, Goudarzi A, Soylak M. Central composite design and genetic algorithm applied for the optimization of ultrasonic-assisted removal of malachite green by ZnO Nanorod-loaded activated carbon. Spectrochim Acta A 2016;167:157–64.

[16] Reis MTA, Freitas OMF, Agarwal S, Ferreira LM, Ismael MRC, Machado R, et al. Removal of phenols from aqueous solutions by emulsion liquid membranes. J Hazard Mater 2011;192:986–94.

[17] Cheng M, Zeng G, Huang D, Cui L, Xu P, Zhang C, et al. Hydroxyl radicals based advanced oxidation processes (AOPs) for remediation of soils contaminated with organic compounds: A review, Chem. Eng. J. 2016; 284:582–598.

[18] Mosleh S, Rahimi MR, Ghaedi M, Dashtian K, Hajati S. $BiPO_4/Bi_2S_3$-HKUST-1-MOF as a novel blue light-driven photocatalyst for simultaneous degradation of toluidine blue and auramine-O dyes in a new rotating packed bed reactor: optimization and comparison to a conventional reactor. RSC Adv 2016;6:63667–80.

[19] Mousavinia SE, Hajati S, Ghaedi M, Dashtian K. Novel nanorose-like Ce(iii)-doped and undoped Cu(ii)-biphenyl-4,4-dicarboxylic acid (Cu(ii)-BPDCA) MOSs as visible light photocatalysts: synthesis, characterization, photodegradation of toxic dyes and optimization. Phys Chem Chem Phys 2016;18:11278–87.

[20] He K, Chen G, Zeng G, Huang Z, Guo Z, Huang T, et al. Applications of white rot fungi in bioremediation with nanoparticles and biosynthesis of metallic nanoparticles. Appl Microbiol Biotechnol 2017:1–10.

[21] Huang Z, Chen G, Zeng G, Chen A, Zuo Y, Guo Z, et al. Polyvinyl alcohol-immobilized *Phanerochaete chrysosporium* and its application in the bioremediation of composite-polluted wastewater, J. Hazard. Mater. 2015;289: 174–183.

[22] Ren X, Zeng G, Tang L, Wang J, Wan J, Liu Y, et al. Sorption, transport and biodegradation - An insight into bioavailability of persistent organic pollutants in soil. Sci Total Environ 2017;610–611:1154–63.

[23] Nandi BK, Goswami A, Purkait MK. Adsorption characteristics of brilliant green dye on kaolin. J Hazard Mater 2009;161:387–95.

[24] Tan X, Liu Y, Zeng G, Wang X, Hu X, Gu Y, et al. Application of biochar for the removal of pollutants from aqueous solutions. Chemosphere 2015;125:70–85.

[25] Azad FN, Ghaedi M, Dashtian K, Hajati S, Pezeshkpour V. Ultrasonically assisted hydrothermal synthesis of activated carbon– HKUST-1-MOF hybrid for efficient simultaneous ultrasound-assisted removal of ternary organic dyes and antibacterial investigation : Taguchi optimization. Ultrason Sonochem 2016;31:383–93.

[26] Jamshidi M, Ghaedi M, Dashtian K, Ghaedi AM, Hajati S, Goudarzi A, et al. Highly efficient simultaneous ultrasonic assisted adsorption of brilliant green and eosin B onto ZnS nanoparticles loaded activated carbon : Artificial neural network modeling and central composite design optimization. Spectrochim Acta A 2016;153:257–67.

[27] Mosleh S, Reza M, Ghaedi M, Dashtian K. Sonochemical-assisted synthesis of CuO / Cu_2O / Cu nanoparticles as e ffi cient photocatalyst for simultaneous degradation of pollutant dyes in rotating packed bed reactor : LED illumination and central composite design optimization. Ultrason Sonochem 2018;40:601–10.

[28] Mosleh S, Rahimi MR, Ghaedi M, Dashtian K, Hajati S. $BiPO_4$/Bi_2S_3-HKUST-1-MOF as a novel blue light-driven photocatalyst for simultaneous degradation of toluidine blue and auramine-O dyes in a new rotating packed bed reactor: optimization and comparison to a conventional reactor. RSC Adv 2016;6:63667–80.

[29] Huang Q, Liu M, Chen J, Wang K, Xu D, Deng F, et al. Enhanced removal capability of kaolin toward methylene blue by mussel-inspired functionalization. J Mater Sci 2016;51:8116–30.

[30] Azad FN, Ghaedi M, Dashtian K, Montazerozohori M, Hajati S, Alipanahpour E. Preparation and characterization of MWCNTs functionalized by

N-(3-nitrobenzylidene)-N′-trimethoxysilylpropyl-ethane-1, 2-diamine for the removal of aluminum (iii) ions via complexation with eriochrome cyanine R: spectrophotometric detection and optimization. RSC Adv 2015;5:61060–9.

[31] Jamshidi M, Ghaedi M, Dashtian K, Hajati S, Bazrafshan A. Ultrasound-assisted removal of Al^{3+} ions and Alizarin red S by activated carbon engrafted with Ag nanoparticles: central composite design and genetic algorithm optimization. RSC Adv 2015;5:59522–32.

[32] Vimonses V, Lei S, Jin B, Chow CWK, Saint C. Adsorption of congo red by three Australian kaolins. Appl Clay Sci 2009;43:465–72.

[33] Huang Q, Liu M, Deng F, Wang K, Huang H, Xu D, et al. Mussel inspired preparation of amine-functionalized Kaolin for effective removal of heavy metal ions. Mater Chem Phys 2016;181:116–25.

[34] He K, Chen G, Zeng G, Chen A, Huang Z, Shi J, et al. Enhanced removal performance for methylene blue by kaolin with graphene oxide modification. J Taiwan Inst Chem Eng 2018;89:77–85.

[35] Lee H, Dellatore SM, Miller WM, Messersmith PB. Mussel-Inspired Surface Chemistry for Multifunctional Coatings. Science 2007;318:426–30.

[36] Cheng C, Li S, Zhao J, Li X, Liu Z, Ma L, et al. Biomimetic assembly of polydopamine-layer on graphene: Mechanisms, versatile 2D and 3D architectures and pollutant disposal. Chem Eng J 2013;228:468–81.

[37] Yan J, Huang Y, Miao YE, Tjiu WW, Liu T. Polydopamine-coated electrospun poly(vinyl alcohol)/poly(acrylic acid) membranes as efficient dye adsorbent with good recyclability. J Hazard Mater 2015;283:730–9.

[38] Zhang S, Zhang Y, Bi G, Liu J, Wang Z, Xu Q, et al. Mussel-inspired

polydopamine biopolymer decorated with magnetic nanoparticles for multiple pollutants removal. J Hazard Mater 2014;270:27–34.

[39] Yu Y, Shapter JG, Popelkafilcoff R, Bennett JW, Ellis A V. Copper removal using bio-inspired polydopamine coated natural zeolites. J Hazard Mater 2014;273:174–82.

[40] He K, Chen G, Zeng G, Peng M, Huang Z, Shi J, et al. Stability, transport and ecosystem effects of graphene in water and soil environments. Nanoscale 2017;9:5370–88.

[41] Ramesha GK, Vijaya Kumara A, Muralidhara HB, Sampath S. Graphene and graphene oxide as effective adsorbents toward anionic and cationic dyes. J Colloid Interface Sci 2011;361:270–7.

[42] Zhang Y, Zeng GM, Lin T, Chen J, Yuan Z, Xiao XH, et al. Electrochemical sensor based on electrodeposited graphene-Au modified electrode and nanoAu carrier amplified signal strategy for attomolar mercury detection. Anal Chem 2015;87:989–96.

[43] Ni Y, Wang W, Huang W, Lu C, Xu Z. Graphene strongly wrapped TiO_2 for high-reactive photocatalyst: a new sight for significant application of graphene. J Colloid Interface Sci 2014;428:162–9.

[44] Zhang M, Gao B, Ying Y, Xue Y, Inyang M. Synthesis, characterization, and environmental implications of graphene-coated biochar. Sci Total Environ 2012;435–436:567–72.

[45] Xu LQ, Yang WJ, Neoh KG, Kang ET, Fu GD. Dopamine-induced reduction and functionalization of graphene oxide nanosheets. Macromolecules 2010;43:8336–9.

[46] Sun L, Yu H, Fugetsu B. Graphene oxide adsorption enhanced by in situ reduction with sodium hydrosulfite to remove acridine orange from aqueous solution. J Hazard Mater 2012;203–204:101–10.

[47] Zhang R, Alecrim V, Hummelgård M, Andres B, Forsberg S, Andersson M, et al. Thermally reduced kaolin-graphene oxide nanocomposites for gas sensing. Sci Rep 2015;5:7676.

[48] Zhao S, Qiu S, Zheng Y, Cheng L, Guo Y. Synthesis and characterization of kaolin with polystyrene via in-situ polymerization and their application on polypropylene. Mater Des 2011;32:957–63.

[49] Zhu L, Lu Y, Wang Y, Zhang L, Wang W. Preparation and characterization of dopamine-decorated hydrophilic carbon black. Appl Surf Sci 2012;258:5387–93.

[50] Hu X, Qi R, Zhu J, Lu J, Luo Y, Jin J, et al. Preparation and properties of dopamine reduced graphene oxide and its composites of epoxy. J Appl Polym Sci 2014;131:39754.

[51] Luo J, Zhao F, Fei X, Liu X, Liu J. Mussel inspired preparation of polymer grafted graphene as a bridge between covalent and noncovalent methods. Chem Eng J 2016;293:171–81.

[52] Li MF, Liu YG, Zeng GM, Liu SB, Hu XJ, Shu D, et al. Tetracycline absorbed onto nitrilotriacetic acid-functionalized magnetic graphene oxide: Influencing factors and uptake mechanism. J Colloid Interface Sci 2017;485:269–79.

[53] Fu J, Chen Z, Wang M, Liu S, Zhang J, Zhang J, et al. Adsorption of methylene blue by a high-efficiency adsorbent (polydopamine microspheres): Kinetics, isotherm, thermodynamics and mechanism analysis. Chem Eng J 2015;259:53–61.

[54] Xu P, Zeng GM, Huang DL, Lai C, Zhao MH, Wei Z, et al. Adsorption of Pb(II) by iron oxide nanoparticles immobilized *Phanerochaete chrysosporium*: Equilibrium, kinetic, thermodynamic and mechanisms analysis. Chem Eng J 2012;203:423–31.

[55] Long F, Gong JL, Zeng GM, Chen L, Wang XY, Deng JH, et al. Removal of phosphate from aqueous solution by magnetic Fe–Zr binary oxide. Chem Eng J 2011;171:448–55.

[56] Auta M, Hameed BH. Chitosan–clay composite as highly effective and low-cost adsorbent for batch and fixed-bed adsorption of methylene blue. Chem Eng J 2014;237:352–61.

[57] Ghosh D, Bhattacharyya KG. Adsorption of methylene blue on kaolinite. Appl Clay Sci 2002;20:295–300.

[58] Gong JL, Wang B, Zeng GM, Yang CP, Niu CG, Niu QY, et al. Removal of cationic dyes from aqueous solution using magnetic multi-wall carbon nanotube nanocomposite as adsorbent. J Hazard Mater 2009;164:1517–22.

[59] Gobi K, Mashitah MD, Vadivelu VM. Adsorptive removal of Methylene Blue using novel adsorbent from palm oil mill effluent waste activated sludge: Equilibrium, thermodynamics and kinetic studies. Chem Eng J 2011;171:1246–52.

[60] Yao Y, Xu F, Chen M, Xu Z, Zhu Z. Adsorption behavior of methylene blue on carbon nanotubes. Bioresour Technol 2010;101:3040–6.

[61] Hoda N, Bayram E, Ayranci E. Kinetic and equilibrium studies on the removal of acid dyes from aqueous solutions by adsorption onto activated carbon cloth. J Hazard Mater 2006;137:344–51.

[62] Hong S, Wen C, He J, Gan FX, Ho YS. Adsorption thermodynamics of Methylene Blue onto bentonite. J Hazard Mater 2009;167:630–3.